Chen *et al.*
Chinese Journal of Mechanical Engineering (2023) 36:57
https://doi.org/10.1186/s10033-023-00887-5

Chinese Journal of Mechanical Engineering

ORIGINAL ARTICLE

Open Access

Experimental Study on Titanium Alloy Cutting Property and Wear Mechanism with Circular-arc Milling Cutters

Tao Chen[1*], Jiaqiang Liu[1], Gang Liu[1], Hui Xiao[1], Chunhui Li[1] and Xianli Liu[1]

Abstract

Titanium alloy has been applied in the field of aerospace manufacturing for its high specific strength and hardness. Nonetheless, these properties also cause general problems in the machining, such as processing inefficiency, serious wear, poor workpiece face quality, etc. Aiming at the above problems, this paper carried out a comparative experimental study on titanium alloy milling based on the CAMC and BEMC. The variation law of cutting force and wear morphology of the two tools were obtained, and the wear mechanism and the effect of wear on machining quality were analyzed. The conclusion is that in contrast with BEMC, under the action of cutting thickness thinning mechanism, the force of CAMC was less, and its fluctuation was more stable. The flank wear was uniform and near the cutting edge, and the wear rate was slower. In the early period, the wear mechanism of CAMC was mainly adhesion. Gradually, oxidative wear also occurred with milling. Furthermore, the surface residual height of CAMC was lower. There is no obvious peak and trough accompanied by fewer surface defects.

Keywords Circular-arc milling cutter, Titanium alloy, Ball-end milling cutter, Surface quality, Milling force, Tool wear, Machining quality

1 Introduction

Titanium alloy is widely applied to the aerospace industry owing to its high strength and hardness, outstanding high and low temperature performance, etc [1, 2]. For example, aircraft engine turbine blades, engine shells and other parts are made of titanium alloy. Yet the titanium alloy is characterized by high chemical reactivity and low elastic modulus [3]. This results in low machining efficiency, severe wear and inferior surface quality in structural parts processing [4, 5]. At present, a ball-end milling cutter (BEMC) is mostly used for machining titanium alloy structural parts. However, the poor machining quality and low milling efficiency of BEMC milling steep surface structural parts had severely restricted the application and promotion of titanium alloys. Therefore, it is an urgent requirement to conduct a study on the development and performance of new structure-cutting tools for the future titanium alloy processing industry.

In the aspect of cutting performance research and structure design of BEMC, Liang et al. [6] conducted the experiment of milling TC17 with cemented carbide BEMC and found that changing the tool cutting direction was conducive to improving the surface residual stress and tool wear. Cheng et al. [7] optimized the design of BEMC by changing the cutter geometrical parameters, and analyzed the variation laws of the optimized cutter milling force by using the finite element method. Chen et al. [8] proposed a mathematical model of a spiral edge

*Correspondence:
Tao Chen
dotnetchen@163.com
[1] School of Mechanical and Power Engineering, Harbin University of Science and Technology, Harbin 150080, China

curve, which overcame the disadvantage of large calculation in the traditional spiral edge modeling approach, and improved the processing efficiency and cutting stability. Zhang et al. [9] combined the bionic structure with BEMC, established a finite element model of the biomimetic BEMC machining process, and studied the variation laws of cutting force. Jin et al. [10] designed two kinds of BEMC with special cutting edges, and carried out milling experiments, which proved that these two kinds of tools can obtain higher machining accuracy and smaller main cutting force in finishing. Antoniadis et al. [11] established the surface morphology and roughness forecasting model of BEMC, and verified the validity of the model through experiments. Abbasi et al. [12] analyzed the influence of the inclination angle of the 5-axes BEMC on the machining deformation of thin-walled parts. The results found that near the angle perpendicular to the workpiece surface, the milling speed and milling force of the cutter were low, which helped to improve the machining accuracy.

Many scholars have also studied the new tool structure for difficult-to-machine materials [13]. Wang et al. [14] presented a revolving cycloid milling cutter with a large spiral angle and front angle. The experiment showed that compared with BEMC, its wear area was shallower and wider, and the processing process produced smaller axial force and tangential force. Song et al. [15] introduced a way to design a variable pitch end milling cutter, and obtained the milling speed range under the stable condition of high-speed milling. Yusoff et al. [16] combined the semi-discretization method with the difference method and proposed the optimal structure of the variable screw cutter and variable pitch cutter. The experimental result showed that the chatter stability of the optimized cutter was improved by 5 times matching with the ordinary cutter. Li et al. [17] developed a barrel ball milling cutter and offered a method to select cutting parameter and calculate tool position. Krishnaraj et al. [13] conducted a high-speed milling experiment of Ti6Al4V with cemented carbide end milling cutter. The results showed that the cutting depth and feed speed had a significant effect on the milling force, and the milling speed had a significant effect on temperature. Chen et al. [18] conducted a comparative experiment of milling TC11 with the self-propelled rotary cutter and indexable cutter. The wear mechanism of self-propelled rotary cutter and its influence on processing performance were obtained.

In summary, related scholars have performed significant research on the milling of titanium alloys with BEMC and ordinary end milling cutters [19–21]. The researches on titanium alloy special integral milling cutters mostly focus on the optimization of tool geometric characteristics and multi-axis machining center toolpath planning [22, 23]. Machining efficiency and tool life are still important factors affecting titanium alloy processing. Compared with BEMC, a circular-arc milling cutter (CAMC) has a larger radius of the cutting edge, which can greatly increase the cutting bandwidth. Besides, the CAMC eliminates the influence of cutter body structure size on cutting edge radius, forming a longer effective cutting edge and improving the utilization rate of tool material. For the purpose of further exploring the milling performance of CAMC, comparative experimental research on titanium alloy milling with BEMC and CAMC was carried out. Combined with milling force, tool wear morphology and machined surface quality, the milling performance of the two kinds of tools was analyzed, which provided theoretical support for the application and popularization of CAMC.

2 Experimental Design

The experimental system is shown in Figure 1. The workpiece material was TC4, and its size was 150 mm×100 mm×30 mm. The machine tool used in the experiment was VDL-1000E high-speed milling center. Furthermore, BEMC and CAMC were installed on it. The substrate materials of the two tools were K88UF cemented carbide with WC as the main component and binder Co accounted for 10%. Both of the tools were coated with AlCrN and the coated layer thickness was 4 μm. The radius of BEMC was 5 mm; the side edge rake angle was 6°; the flank angle was 12°, and the helix angle was 30°. The radius of CAMC was 5 mm; the end edge radius was 9 mm; the side edge radius was 45 mm; the rake angle was 6°; the flank angle was 12°, and the helical angle of the helical groove was 30°.

The experimental parameters shown in Table 1 were designed to investigate the impact of machining parameters on the cutting force. The side milling process was conducted in the down milling with BEMC and CAMC respectively. The data on cutting force was collected by the Kistler 9139AA dynamometer.

For fear of the deviation of experimental results due to extreme parameters, the processing parameters were fixed: milling speed 70 m/min, feed per tooth 0.06 mm/z, cutting width 0.3 mm. Each time when the milling distance reached 30 m, the tools were removed. The SU3500 scanning electron microscope was employed to detect the flank wear morphology of BEMC and CAMC. Then the wear area was analyzed by Bruker xflash6|30 energy spectrometer. Meanwhile, after unloading the workpiece, workpiece face quality was detected by the Talysurf CCI white-light interferometer. The surface roughness was characterized by S_q, the root mean square deviation of the surface contour height.

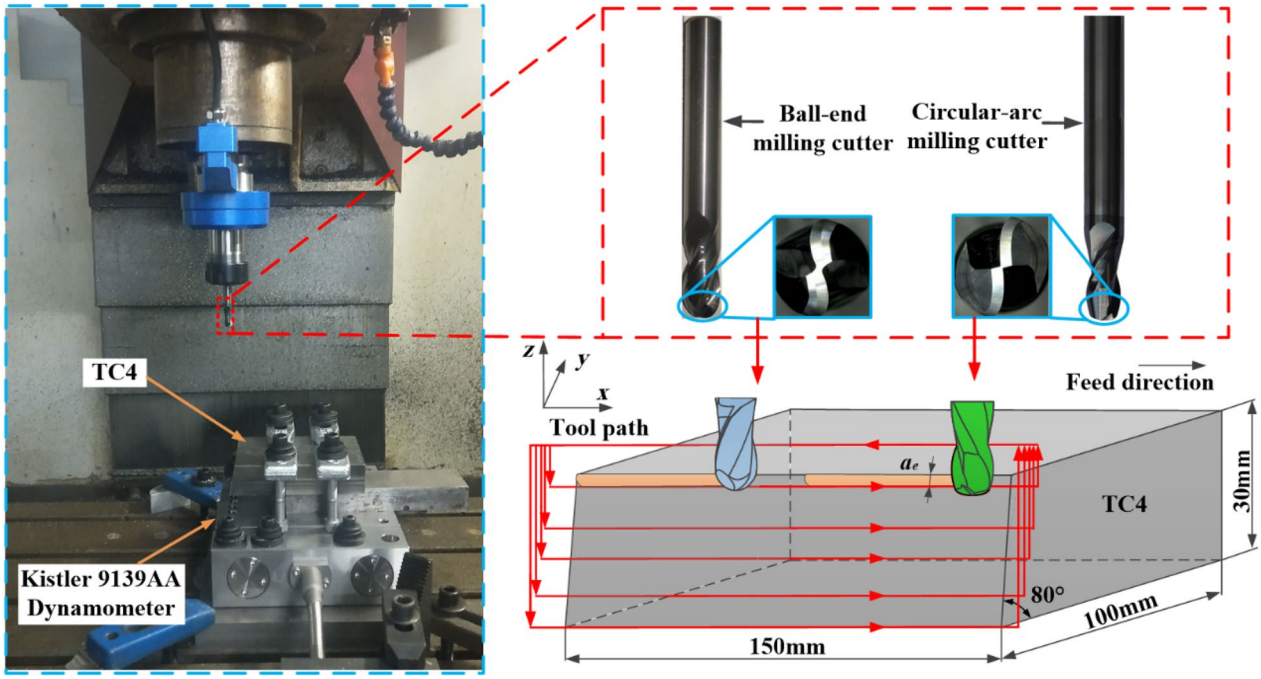

Figure 1 Experimental system

Table 1 Experimental parameters

Serial number	Speed (V_c) (m/min)	Feed per tooth (f_z) (mm/z)	Width (a_e) (mm)	Tools
Nos. 1–8	50, 70, 90, 110	0.06	0.3	BEMC CAMC
Nos. 9–14	70	0.04, 0.08, 0.10	0.3	
Nos. 15–20	70	0.06	0.1, 0.2, 0.4	

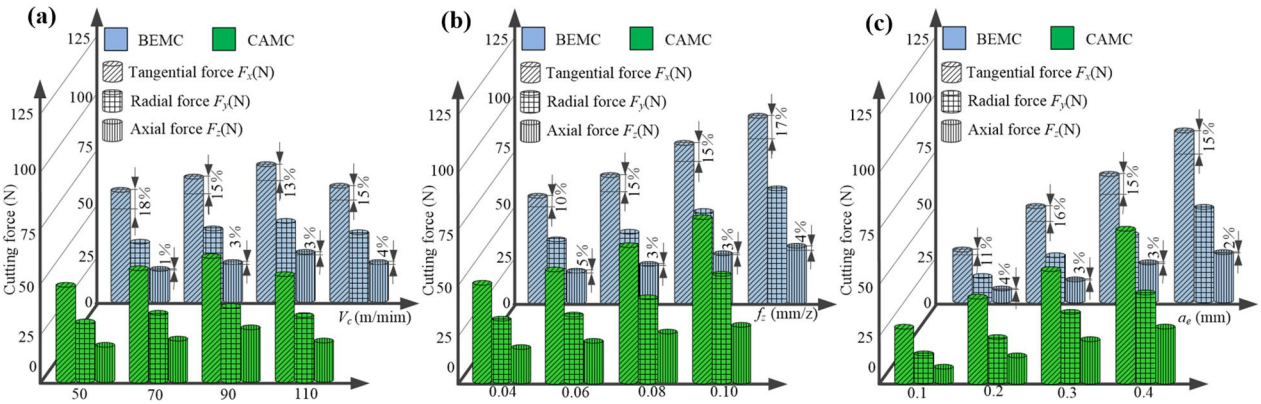

Figure 2 Variation law of cutting force with milling parameters: **a** Milling speed, **b** Feed per tooth and **c** Cutting width

3 Analysis of Experimental Results

3.1 Analysis of Milling Forces

The forces variation law of two kinds of tools with milling speed, feed per tooth and cutting width was shown in Figure 2. As can be seen from the figure, the forces change trend of the two tools with the milling speed was basically the same, which increased with the milling speed increasing and decreased gradually when the

milling speed was more than 90 m/min. At the same time, the growth of feed per tooth and cutting width increased the cutting resistance, and the milling forces in all directions of both tools also enlarged significantly. Because of the larger radius side edge, the narrower cutting region of CAMC reduced the cutting thickness and the milling force. When the cutting volume enlarged, the effect of reducing the milling force was more outstanding. The forces of CAMC were less than that of BEMC, especially the tangential force F_x was about 15% smaller than that of BEMC, while the axial force F_z of CAMC was not significantly lower than that of BEMC. The F_z of CAMC was only 4% lower than that of BEMC with feed per tooth 0.10 mm/z. The reason is that the different helix angles in the cutting area of tools can result in different force decomposition effects. This led to the different proportions of the forces in all directions between BEMC and CAMC.

Figure 3 shows the actual measured data of tangential force F_x of the two kinds of tools at a milling speed of 70 m/min, feed per tooth of 0.06 mm/z, and cutting width of 0.3 mm. It can be seen that the F_x peak value of BEMC was higher than that of CAMC, and the former F_x peak value fluctuation range was also greater than that of the latter. This can be interpreted as CAMC relieving the fluctuation of the cutting force caused by the frictional resistance and mechanical shock concentration for its flat cutting edge. Thus the processing stability was higher.

3.2 Analysis of Tool Wear Process and Mechanism

Figure 4 shows the flank wear morphology in different milling lengths. It is observed that the adhesive layer appeared on the flank of BEMC and CAMC obviously at a milling length of 60 m. Since the strong affinity of titanium alloy, the cutting area of the flank face

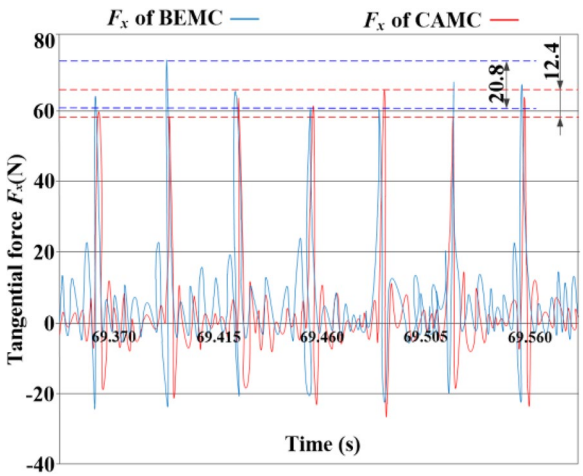

Figure 3 Actual measured data of tangential force F_x

formed a bonding under friction. But the difference is that the bonding of BEMC was relatively concentrated and blocky, while the flank adhesive layer of CAMC was more uniform. Moreover, its width was smaller than that of BEMC and appeared as a strip.

As the milling progressed, the extrusion and friction between the tool and the workpiece intensified, which led to a degradation in cutting performance. When the machining length reached 150 m, the bonding on the cutting edge of BEMC fell off constantly, which weakened the cohesion between the coating and substrate. Furthermore, because of the large curvature transformation of the cutting edge, the force on both sides and the middle of the cutting edge was uneven. Therefore, under the action of mechanical and thermal shock, micro notches occurred at the weak part. At this period, the flank adhesive layer of CAMC also fell off continuously, forming a strip-shaped wear belt with intermittent coating. However, the flatter cutting edge of CAMC made the contact between the flank face and the machined surface more uniform, and thereby avoided tool tipping. As the milling length reached 240 m, the gradually increasing stress on the cutting edge of BEMC accelerated the separation of substrate material particles, and there was tool tipping on the cutting edge. Although tiny tipping also appeared on CAMC, they were smaller and more dispersed than those of BEMC, and the cutting edge remained relatively intact.

Figure 5a and b shows the flank wear morphology of BEMC and CAMC at the machining length of 60 m. It can be seen that the two kinds of tools had different degrees of bonding. Due to the concentration of the cutting area, under high stress and high temperature, there was a large bonding on the flank of BEMC. The wear area was not uniform, and some coating was removed nearby. At this point, block bonding appeared at the cutting edge of CAMC. And strip adhesive layer appeared at the bottom of the block bonding, which was evenly coated on the tool surface. Compared with BEMC, CAMC had smaller block bonding and a narrower tool wear area.

When the machining length reached 150 m, the bonding at the cutting edge of BEMC increases, and a large area of coating peeling occurred, exposing the tool substrate (Figure 5c). O and Ti were found by the analysis of the material composition. This showed that the tool oxidative wear occurred, and the Ti diffused into the tool with the increase of temperature. The TiC layer, which formed by C in the tool and Ti, and adhered to the tool surface, was continuously worn away under the cyclic impact force. Bonding tear characterized by bonding pits has formed, which reduced tool substrate strength and increased tool wear. Meanwhile, the bonding debris on CAMC continuously peeled off and took away the

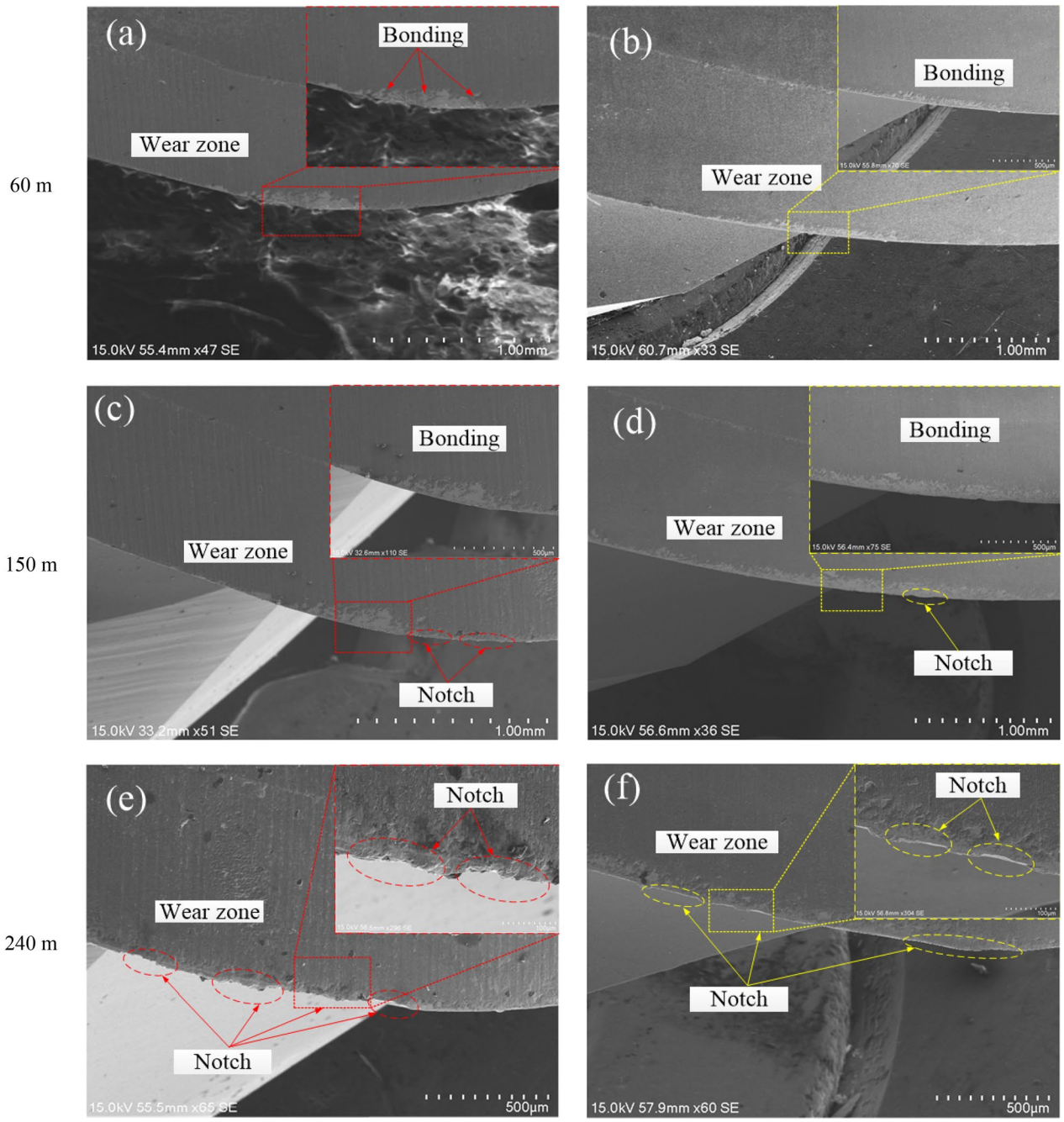

Figure 4 Flank wear morphology

coating, and the wear area presented a uniform strip shape (Figure 5d). Furthermore, a large amount of Al, N and Cr were detected in the wear area, which indicated that the coating was not completely peeled off and in a slow grinding process. It can be deduced that CAMC was in a stable wear period. Additionally, a small amount of O was found in the cutting area, and thus CAMC also had slight oxidation wear.

Figure 5e and f shows the flank wear morphology of two tools at the machining length of 240 m. There was tipping at the cutting edge of BEMC, and a tight adhesive layer was found in these areas. It indicated that tool tipping had occurred at an earlier time. Further

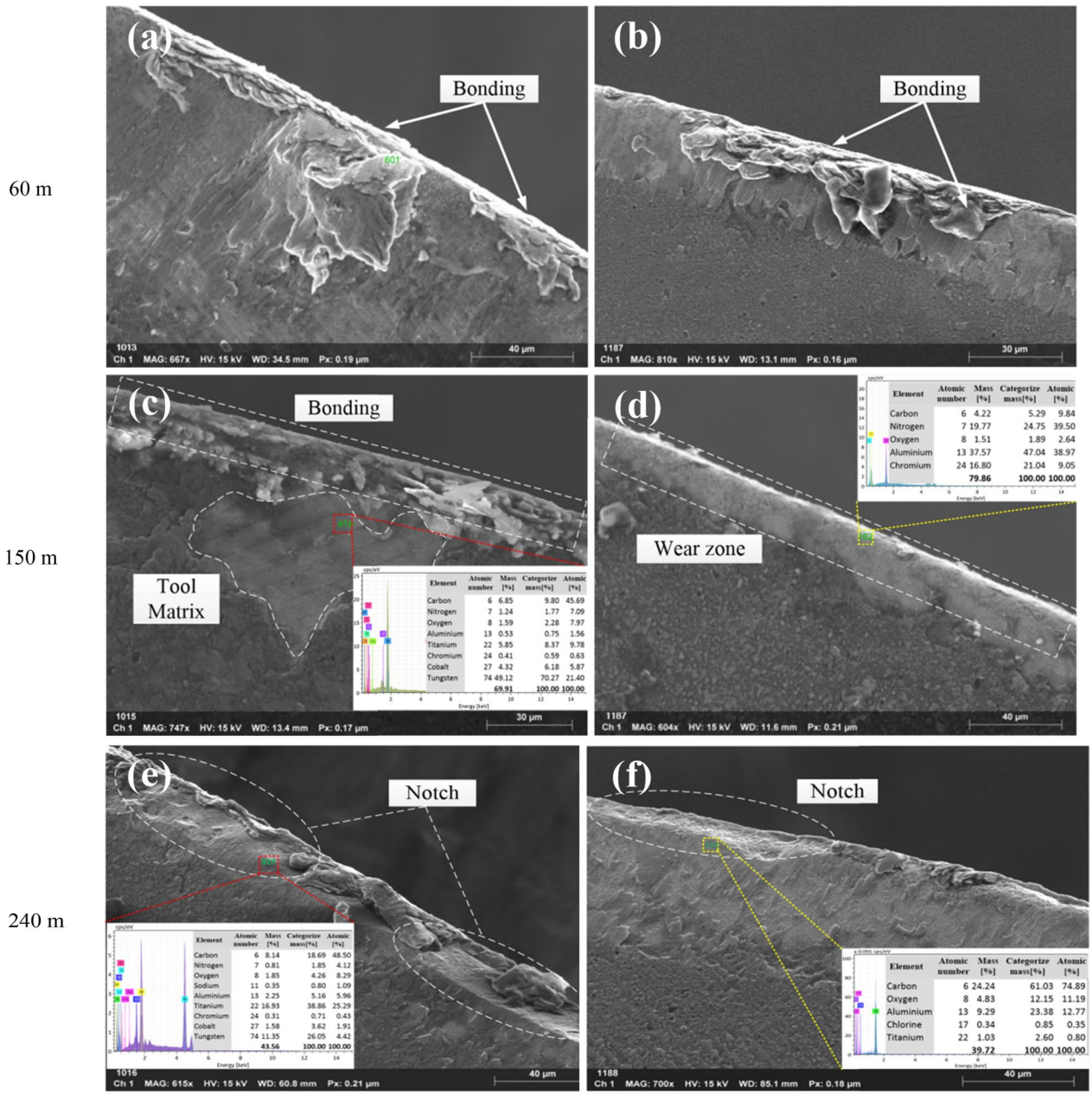

Figure 5 Flank wear morphology at different length

elemental analysis results of the wear area show that the content of C increases and the content of Co decreases at the cutting edge. At this time, the diffusion of Co to the inside led to a lack on the surface, resulting in a decrease in the bonding strength between the substrate C particles. So the substrate material fell off together with the bonding, which was the main reason for the formation of severe tool tipping. In this period, the coating peeling of CAMC intensified, and the width of the wear area increased. Additionally, there was a small amount of adhesive layer and tiny notches occurred at the same time. However, since the flank face of CAMC contacted the workpiece more evenly, the heat dissipation conditions were improved while reducing friction. Therefore, the spalling of the tool substrate was avoided. The energy spectrum analysis showed that the

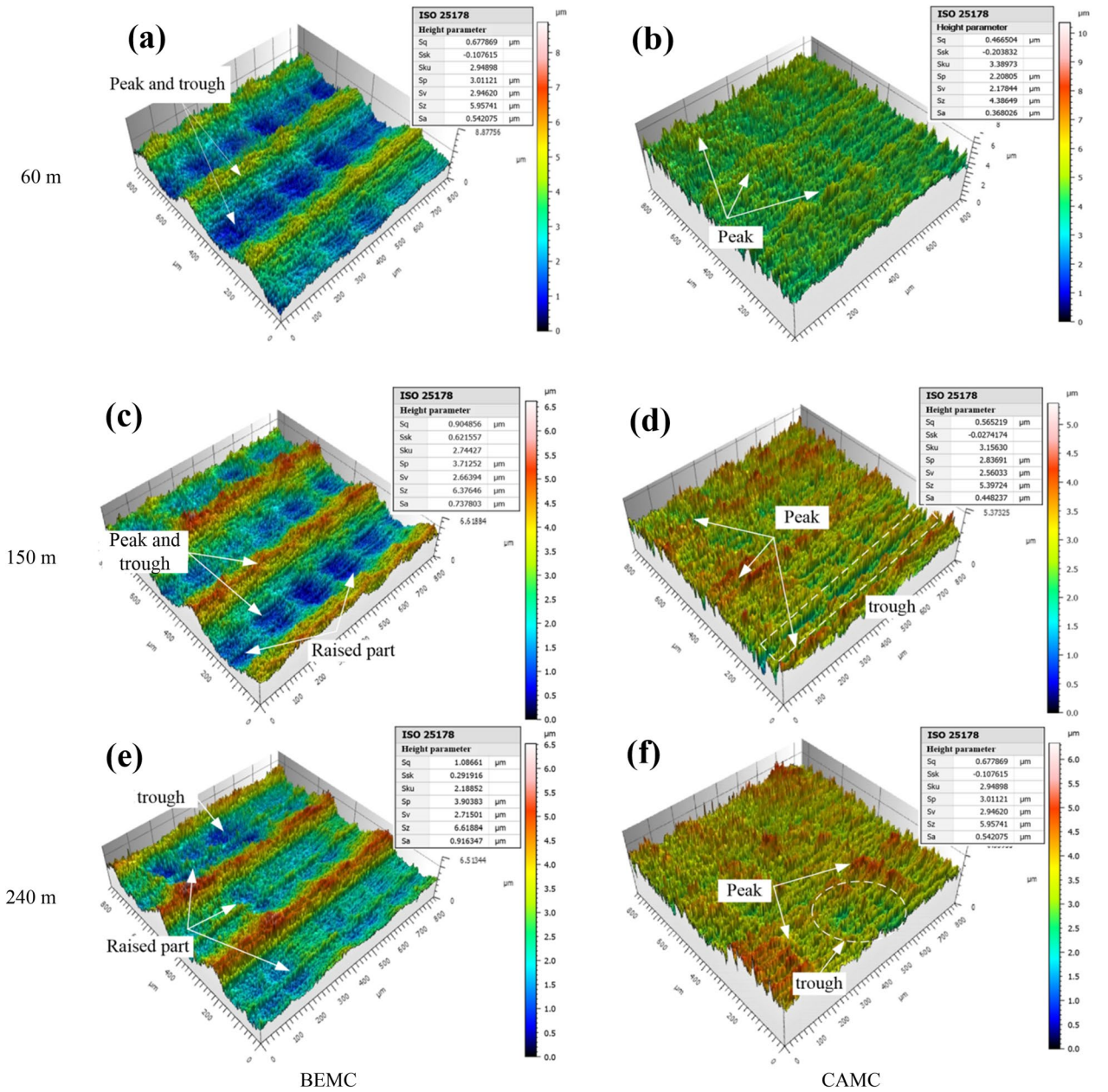

Figure 6 Comparison of the machined surface morphology at different length

content of O increased and there was a small amount of Ti at the tipping area. This showed that oxidative wear and slight diffusion wear occurred at the same time.

3.3 Effect of Tool Wear on Surface Quality

Figure 6a and b shows the comparison of the machined surface morphology at the machining length of 60 m. It can be observed that an outstanding peak and trough appeared on the surface machined by BEMC, and the S_q was 0.679 μm. Due to the small radius of the ball head, BEMC cut into the workpiece and produced obvious ball pits in the wave trough. In contrast with BEMC, CAMC had a flatter machining surface, with only shallow strip grooves and slight wave crests. Its S_q was 0.467 μm and smaller than that of BEMC.

When the machining length was 150 m, the two kinds of tools entered into a stable wear stage. At this point, the wear of BEMC was relatively severe. The peak and trough of the machined surface were more remarkable, and reflected in the wave peak height increasing. The

maximum height of the peak top S_p was 3.713 μm. Concurrently the defects at the cutting edge were reflected on the machining surface, and there were bulges along the feed direction at the trough floor (Figure 6c). The wave peak on the machining surface of CAMC had also begun to become prominent, and a narrow trough had appeared. Compared with BEMC, its surface quality had not significantly decreased. The S_q was 0.565 μm, which was much smaller than 0.905 μm of BEMC (Figure 6d).

As the machining length increased, continuous abrasion and mechanical shock between BEMC and the workpiece led to tool tipping and intensified the squeeze plowing action. Therefore, when the machining length was 240 m, the bulge on the surface was more outstanding, and the ball pit in the wave trough became irregular and more rugged. The peak height increased further, and the S_q reached 1.087 μm (Figure 6e). The surface quality machined by CAMC also dropped to some degree. The uniform wave peak disappeared and was replaced by an irregular wave peak and shallow trough. These phenomena were caused by the notches of CAMC and the decrease of machining stability. By contrast, the S_q value of CAMC was only 0.678 μm, so the surface quality was better (Figure 6f).

3.4 Analysis and Discussion of Cutting State

According to the above, the residual height value of CAMC was lower, and the surface quality was better. This paper analyzed the actual processing situation of BEMC and CAMC, and established the mathematical model of residual height. Figure 7 shows the comparison of machined surface residual height after milling by BEMC and CAMC. The residual height of machined surface h is:

$$h = R - \frac{\sqrt{4R^2 - L^2}}{2}, \tag{1}$$

where R is the radius of the cutting edge, L the processing line spacing.

As can be seen from Figure 7, under the condition of the same processing line spacing and milling width, the larger radius cutting edge of CAMC cut into the workpiece, resulting in more uniform thickness and thinner average cutting thickness. Moreover, it can be seen from Eq. (1) that the surface residual height h at the two adjacent tool paths overlap of CAMC is lower under the condition of fixed processing row spacing L. Thus the surface quality is improved.

To investigate the milling forces of the two kinds of tools, it is indispensable to create the milling force model diagram in the normal plane reference frame based on the actual cutting process (Figure 8). The cutting area is equivalent to point A. At point A, the cutting edge receives a feed force F_c perpendicular to the base plane P_r and a tangential force F_t directed to the cutting edge center in the normal section P_n. The resultant shear force F of these two forces can be expressed as follows.

$$F = \frac{\tau_s \cdot a_e \cdot H_D}{\sin\phi \cdot \cos(\phi + \eta - \gamma')}, \tag{2}$$

where τ_s stands for the shear stress, a_e the cutting width, H_D the instantaneous undeformed cutting thickness, ϕ the shear angle, γ' working rake angle, η the friction angle determined by the experiment.

Taking into account the differences in cutting performance caused by different cutting areas of the tool, it is necessary to probe the impact of the geometric characteristics on helix angle β. The cutting area of CAMC is the side edge, and its helix angle is 30°. The cutting area of BEMC is the end edge, both its equivalent helix angle β' and working rake angle γ' measured in main section P_n vary with the axial position angle θ of point A, as is shown in the following equations.

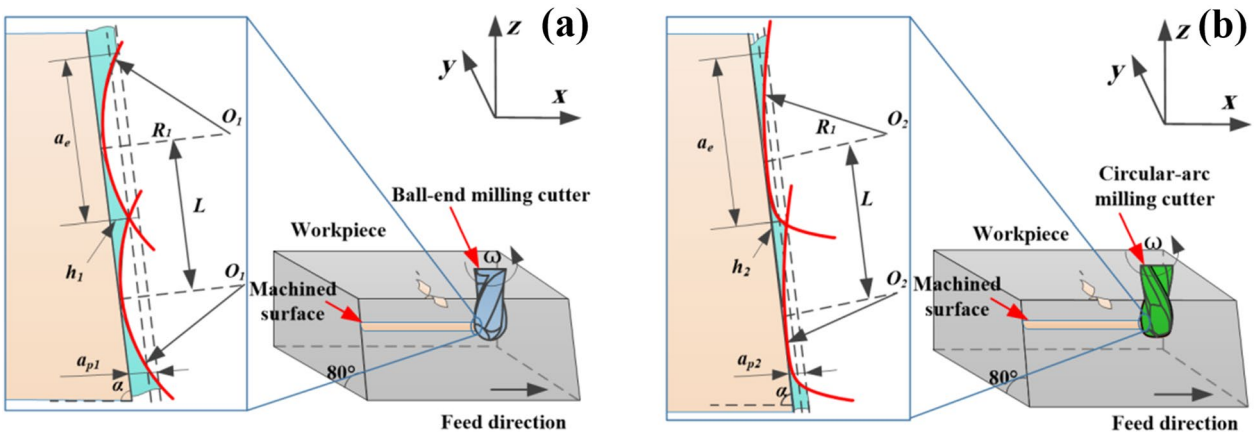

Figure 7 Comparison of machined surface residual height: **a** BEMC and **b** CAMC

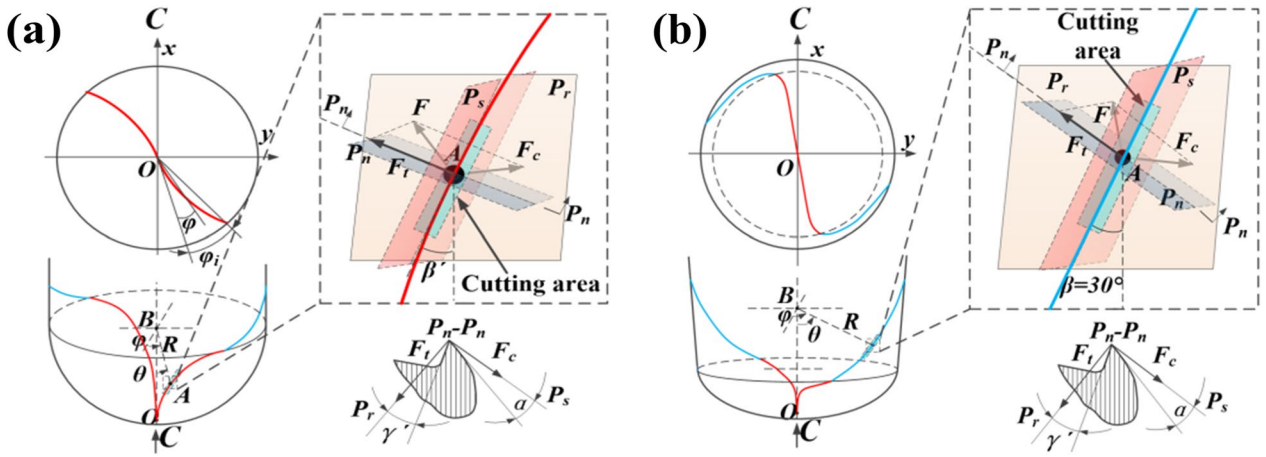

Figure 8 Milling force model diagram: **a** BEMC and **b** CAMC

$$\beta' = \arccos\left(\frac{\cot\beta}{\sqrt{(\sin\theta)^4 + (\cot\beta)^2}}\right), \tag{3}$$

$$\gamma' = sin\gamma\cos^2\beta' + \sin^2\beta'. \tag{4}$$

According to Eq. (3), the end edge equivalent helix angle of BEMC increases nonlinearly with the axial position angle θ and is less than the helix angle of CAMC by 30°. Compared with BEMC, constant helix angle of the side edge of CAMC makes the cutting process more stable. Moreover, the larger helix angle can effectively decompose the main cutting force into axial direction, which makes the axial force component increase significantly. This is the reason that the decline of F_x and F_y of CAMC is more remarkable than that of F_z (Figure 8). Eq. (4) demonstrates that the working rake angle γ' of CAMC is larger, which will be mentioned in the calculation of the cutting force later.

The other parameters in Eq. (2) can be expressed as:

$$H_{D\max} = \frac{\sqrt{4R^2 - a_e^2}}{2\sin\left[\arctan\left(\frac{\sqrt{4R^2-a_e^2}}{a_e-2f_z}\right)\right]}, \tag{5}$$

$$\phi = \frac{\pi}{4} - \frac{\eta - \gamma'}{2}. \tag{6}$$

Therefore, the maximum shearing force F_{max} of a single cutting edge in the cutting process can be obtained.

$$F_{\max} = \frac{\tau_s \cdot a_e \cdot \sqrt{4R^2 - a_e^2}}{2\sin\left[\arctan\left(\frac{\sqrt{4R^2-a_e^2}}{a_e-2f_z}\right)\right] \cdot \sin\left(\frac{\pi}{4} - \frac{\eta-\gamma'}{2}\right) \cdot \cos\left(\frac{\pi}{4} + \frac{\eta-\gamma'}{2}\right)}. \tag{7}$$

It can be seen from Eq. (5) that CAMC reduces the maximum instantaneous cutting thickness H_{Dmax} for its larger side edge radius R. Therefore, the conclusion can be drawn from Eq. (7) that the large working rake angle of CAMC and the cutting thickness thinning mechanism reduce the maximum cutting force during the cutting process jointly. Furthermore, the tool wear was effectively relieved. It is worth noting that the larger radius and flatter cutting edge of CAMC make the wear area dispersed and uniform to avoid heat concentration. Consequently, this also has a positive effect on prolonging tool life.

4 Conclusions

In this paper, the cutting property comparison study of ball-end milling cutters (BEMC) and circular-arc milling cutters (CAMC) was carried out. The comparative analysis was made of milling forces, tool wear and surface quality. The following conclusions were obtained.

(1) In contrast with BEMC, the tangential force and radial force decreased obviously under the action of cutting thickness thinning mechanism. In addition, the tangential force fluctuation amplitude of CAMC was significantly smaller than that of BEMC, which represented excellent dynamic processing performance.
(2) The flank face of CAMC was dominated by adhesive wear, and the wear area was near the cutting

edge and narrower. After a long cutting time, obvious oxidation wear was observed. The width and depth of the wear area increased slowly. The final failure occurred with the appearance of the notches.

(3) In the whole cutting process, CAMC had better surface quality. There was no obvious peak and trough in machined surface, and the surface roughness S_q was kept at a low level.

(4) The machined surface produced by CAMC had lower residual height under the action of a large cutting edge radius. Compared with BEMC, the large working rake angle of CAMC and the reduction of cutting thickness decreased the maximum cutting force. And the flatter cutting edge makes the heat even, effectively relieving tool wear.

Acknowledgements
Not applicable.

Author Contributions
TC has organized the project, designed the experiments, and written the manuscript; JL has conducted the experiments, and collected and analyzed data; GL has designed the experiments, analyzed and arranged data, and written the manuscript; HX has conducted the experiments, and collected and analyzed data; CL has reviewed the manuscript; XL has reviewed the manuscript. All authors read and approved the final manuscript.

Authors' Information
Tao Chen, born in 1979, is currently a professor and a PhD candidate supervisor at *Key Laboratory of Advanced Manufacturing and Intelligent Technology, Ministry of Education, Harbin University of Science and Technology, China*. He received his PhD degree from *Harbin University of Science and Technology, China*, in 2009. His main research interests include milling technology and equipment, tool design and manufacturing, intelligent control.
Jiaqiang Liu, born in 1993, is currently a doctoral candidate at *Key Laboratory of Advanced Manufacturing and Intelligent Technology, Ministry of Education, Harbin University of Science and Technology, China*.
Gang Liu, born in 1997, is currently a master candidate at *Key Laboratory of Advanced Manufacturing and Intelligent Technology, Ministry of Education, Harbin University of Science and Technology, China*.
Hui Xiao, born in 1993, is currently a doctoral candidate at *Key Laboratory of Advanced Manufacturing and Intelligent Technology, Ministry of Education, Harbin University of Science and Technology, China*.
Chunhui Li, born in 1996, is currently a doctoral candidate at *Key Laboratory of Advanced Manufacturing and Intelligent Technology, Ministry of Education, Harbin University of Science and Technology, China*.
Xianli Liu, born in 1961, is currently a professor and a PhD candidate supervisor at *Key Laboratory of Advanced Manufacturing and Intelligent Technology, Ministry of Education, Harbin University of Science and Technology, China*. His main research interests include clean cutting, multimedia cutting database and image technology.

Funding
Supported by National Natural Science Foundation of China (Grant No. 51975168).

Availability of Data and Materials
All data generated or analysed during this study are included in this published article.

Declarations

Competing Interests
The authors declare no competing financial interests.

Received: 17 January 2022 Revised: 9 April 2023 Accepted: 14 April 2023
Published online: 28 April 2023

References

[1] A Pramanik. Problems and solutions in machining of titanium alloys. *The International Journal of Advanced Manufacturing Technology*, 2014, 70(5–8): 919–928.
[2] C Veiga, J P Davim, A J R Loureiro. Review on machinability of titanium alloys: The process perspective. *Reviews on Advanced Materials Science*, 2013, 34(2): 148–164.
[3] W Polini, S Turchetta. Cutting force, tool life and surface integrity in milling of titanium alloy Ti-6Al-4V with coated carbide tools. *Proceedings of the Institution of Mechanical Engineers*, *Part B*: *Journal of Engineering Manufacture*, 2016, 230(4): 694–700.
[4] H Jung, T Hayasaka, E Shamoto, et al. Suppression of forced vibration due to chip segmentation in ultrasonic elliptical vibration cutting of titanium alloy Ti–6Al–4V. *Precision Engineering*, 2020, 64: 98–107.
[5] Z G Wang, Y S Wong, M Rahman. High-speed milling of titanium alloys using binderless CBN tools. *International Journal of Machine Tools & Manufacture*, 2005, 45(1): 105–114.
[6] T Liang, C Yao, J Ren, et al. Effect of cutter path orientations on cutting forces, tool wear, and surface integrity when ball end milling TC17. *The International Journal of Advanced Manufacturing Technology*, 2017, 88(9–12): 2589–2602.
[7] Y N Cheng, S An, X L Liu, et al. Experimental study and simulation analysis on ball-end cutter milling titanium alloy based on the geometric parameters optimization. *Key Engineering Materials*, 2014, 589–590: 427–432.
[8] X Chen, G Ding, R Li, et al. A new design and grinding algorithm for ball-end milling cutter with tooth offset center. *Proceedings of the Institution of Mechanical Engineers*, *Part B*: *Journal of Engineering Manufacture*, 2014, 228(7): 687–697.
[9] W Zhang, L Zhang, B Wang, et al. Finite element simulation analysis of bionic ball-end milling cutter. *The International Journal of Advanced Manufacturing Technology*, 2019, 103(5–8): 3151–3161.
[10] M Jin, I Goto, T Watanabe, et al. Development of CBN ball-nosed end mill with newly designed cutting edge. *Journal of Materials Processing Technology*, 2007, 192–193: 48–54.
[11] A Antoniadis, C Savakis, N Bilalis, et al. Prediction of surface topomorphy and roughness in ball-end milling. *The International Journal of Advanced Manufacturing Technology*, 2003, 21(12): 965–971.
[12] S A Abbasi, P F Feng, Y Ma, et al. Finite element deformation analysis of long thin cantilever shape parts in high speed ball end milling of titanium alloy Ti-6Al-4V with PCD tools at various tool inclination angles. *Key Engineering Materials*, 2016, 693: 1038–1045.
[13] V Krishnaraj, S Samsudeensadham, R Sindhumathi, et al. A study on high speed end milling of titanium alloy. *Procedia Engineering*, 2014, 97: 251–257.
[14] G Y Wang, X L Liu, T Chen, et al. An experimental study on milling titanium alloy with a revolving cycloid milling cutter. *Applied Sciences*, 2020, 10(4): 1423–1434.
[15] Q Song, X Ai, J Zhao. Design for variable pitch end mills with high milling stability. *The International Journal of Advanced Manufacturing Technology*, 2011, 55(9–12): 891–903.
[16] A R Yusoff, N D Sims. Optimisation of variable helix tool geometry for regenerative chatter mitigation. *International Journal of Machine Tools and Manufacture*, 2011, 51(2): 133–141.
[17] T Li, W Y Chen, R F Xu, et al. Flank milling for blisk with a barrel ball milling cutter. *Key Engineering Materials*, 2009, 407–408: 202–206.
[18] T Chen, Y S Wang, W J Gao, et al. Comparative study on the cutting performance of self-propelled rotary cutters and indexable cutters in milling TC11 titanium alloy. *The International Journal of Advanced Manufacturing Technology*, 2020, 111(9): 2749–2758.
[19] Q Shi, L Li, N He, et al. Experimental study in high speed milling of titanium alloy TC21. *The International Journal of Advanced Manufacturing Technology*, 2016, 64(1–4): 49–54.

[20] A K M N Amin, A F Ismail, M K N Khairusshima. Effectiveness of uncoated WC-Co and PCD inserts in end milling of titanium alloy-Ti-6Al-4V. *Journal of Materials Processing Tech*, 2007, 192–193: 147–158.
[21] H H Su, P Liu, Y C Fu, et al. Tool life and surface integrity in high-speed milling of titanium alloy TA15 with PCD/PCBN tools. *Chinese Journal of Aeronautics*, 2012, 25(5): 784–790.
[22] D Yan, D Zhang, M Luo. Optimization of barrel cutter for five-axis flank-milling based on approximation of tool envelope surface. *Computer Aided Design & Applications*, 2015, 12(6): 717–722.
[23] M Luo, D Q Yan, B H Wu, et al. Barrel cutter design and toolpath planning for high-efficiency machining of freeform surface. *The International Journal of Advanced Manufacturing Technology*, 2016, 85(9–12): 2495–2503.